NAVAL POSTGRADUATE SCHOOL
Monterey, California

THESIS

EFFECTS OF WATER VAPOR AND ANISOTROPIC SCATTERING ON AEROSOL OPTICAL DEPTH RETRIEVAL

by

Mary B. Clifford

December 1991

Thesis Advisor Philip A. Durkee

DISCLAIMER NOTICE

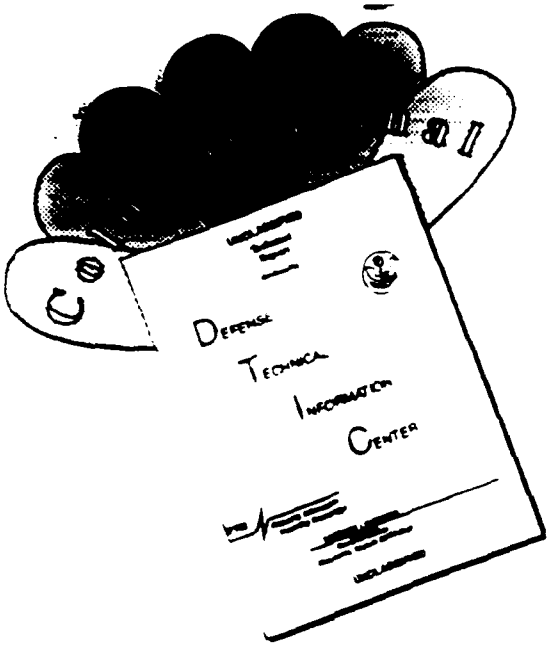

THIS DOCUMENT IS BEST QUALITY AVAILABLE. THE COPY FURNISHED TO DTIC CONTAINED A SIGNIFICANT NUMBER OF COLOR PAGES WHICH DO NOT REPRODUCE LEGIBLY ON BLACK AND WHITE MICROFICHE.

Unclassified

security classification of this page

REPORT DOCUMENTATION PAGE

1a Report Security Classification: Unclassified			1b Restrictive Markings
2a Security Classification Authority			3 Distribution Availability of Report: Approved for public release; distribution is unlimited.
2b Declassification Downgrading Schedule			
4 Performing Organization Report Number(s)			5 Monitoring Organization Report Number(s)
6a Name of Performing Organization: Naval Postgraduate School	6b Office Symbol (*if applicable*): 35		7a Name of Monitoring Organization: Naval Postgraduate School
6c Address (*city, state, and ZIP code*): Monterey, CA 93943-5000			7b Address (*city, state, and ZIP code*): Monterey, CA 93943-5000
8a Name of Funding Sponsoring Organization	8b Office Symbol (*if applicable*)		9 Procurement Instrument Identification Number
8c Address (*city, state, and ZIP code*)			10 Source of Funding Numbers: Program Element No / Project No / Task No / Work Unit Accession No

11 Title (*include security classification*)
EFFECTS OF WATER VAPOR AND ANISOTROPIC SCATTERING ON AEROSOL OPTICAL DEPTH RETRIEVAL

12 Personal Author(s): Mary B. Clifford

13a Type of Report	13b Time Covered	14 Date of Report (*year, month, day*)	15 Page Count
Master's Thesis	From To	December 1991	48

16 Supplementary Notation: The views expressed in this thesis are those of the author and do not reflect the official policy or position of the Department of Defense or the U.S. Government.

17 Cosati Codes			18 Subject Terms (*continue on reverse if necessary and identify by block number*)
Field	Group	Subgroup	word processing, Script, GML, text processing.

19 Abstract (*continue on reverse if necessary and identify by block number*)

NOAA-7 AVHRR data from April 1982 was used to perform global-scale analysis of aerosol particle characteristics. Mahony's (1991) water vapor correction was incorporated into the AVHRR multichannel satellite data processing technique used by Frost (1988). Channel 4 Channel 5 brightness temperature difference was used as an estimate of water vapor content in an air column. Greatest measured water vapor content was at the equator, decreasing toward the poles. Applying the correction reduced the aerosol particle size index, resulting in an increase in aerosol optical depths. In addition, the high particle size index over the low latitudes in the southern hemisphere noted by Frost, was reduced significantly after applying the correction. A comparison was made between Frost's values for the variable two-term Henyey-Greenstein phase function and those derived with the water vapor correction. The basic shape of the curve is similar to that determined by Frost.

20 Distribution Availability of Abstract: ☒ unclassified unlimited ☐ same as report ☐ DTIC users	21 Abstract Security Classification: Unclassified	
22a Name of Responsible Individual: Philip A. Durkee	22b Telephone (*include Area code*): (408) 646-3465	22c Office Symbol: MR Dc

DD FORM 1473,84 MAR 83 APR edition may be used until exhausted
All other editions are obsolete

security classification of this page

Approved for public release; distribution is unlimited.

Effects of Water Vapor and Anisotropic Scattering on Aerosol Optical Depth Retrieval

by

Mary B. Clifford
Lieutenant, United States Navy
B.S., State Univeristy of New York at Albany, 1979

Submitted in partial fulfillment of the
requirements for the degree of

MASTER OF SCIENCE IN METEOROLOGY AND PHYSICAL OCEANOGRAPHY

from the

NAVAL POSTGRADUATE SCHOOL
December 1991

Author: Mary B Clifford
Mary B. Clifford

Approved by:
Philip A. Durkee, Thesis Advisor

Patricia M. Pauley
Patricia M. Pauley, Second Reader

Robert L Haney
Robert L. Haney, Chairman,
Department of Meteorology

ABSTRACT

NOAA-7 AVHRR data from April 1982 was used to perform global-scale analysis of aerosol particle characteristics. Mahony's (1991) water vapor correction was incorporated into the AVHRR multichannel satellite data processing technique used by Frost (1988). Channel 4/Channel 5 brightness temperature difference was used as an estimate of water vapor content in an air column. Greatest measured water vapor content was at the equator, decreasing toward the poles. Applying the correction reduced the aerosol particle size index, resulting in an increase in aerosol optical depths. In addition, the high particle size index over the low latitudes in the southern hemisphere noted by Frost, was reduced significantly after applying the correction. A comparison was made between Frost's values for the variable two-term Henyey-Greenstein phase function and those derived with the water vapor correction. The basic shape of the curve is similar to that determined by Frost.

TABLE OF CONTENTS

LIST OF TABLES

LIST OF FIGURES

ACKNOWLEDGEMENTS

For all the effort that has gone into this endeavor, a lot of support and help have come from a number of individuals. First and foremost, my heartfelt thanks to the two individuals whose assistance was instrumental in all aspects of this thesis -- Professor Philip Durkee whose patience and ability to understand difficult circumstances reassured me that nothing was insurmountable and Mr. Craig Motell for his programming wizardry and lively sense of humor. For the support I received from Fleet Numerical Oceanography Center personnel -- "Muchas Gracias"; particularly to Captain J. J. Jensen, Captain B. Edwards, and most especially to all the Command Duty Officers who took the watch to allow me to complete my course work. Finally, to the two individuals who have shared "the heartache and the victory", Lieutenant Teri Egger and Lieutenant Brian Miller; your support was always appreciated, if not always expressed.

I. INTRODUCTION

A. PURPOSE

The availability of satellite-measured radiances provides an effective and relatively inexpensive means for determining aerosol particle distribution on a global scale. Satellites provide extensive coverage of the earth's surface with sufficient temporal periodicity to allow for the study of large-scale global effects while at the same time providing small-scale local measurements desirable for military applications. Data from meteorological satellites require careful processing in order to distinguish the much lower radiances associated with aerosol optical depth variations (Durkee 1984) from the greater radiances associated with cloud albedos, satellites were designed to measure.

Improved aerosol optical depth retrieval algorithms have facilitated ongoing efforts to establish a global aerosol particle data base. Frost (1988) developed an algorithm to derive aerosol particle characteristics from the Advanced Very High Resolution Radiometer (AVHRR) on NOAA polar orbiting satellites. Aerosol particle size index can be derived by a comparison of the sensitivities of two adjacent spectral windows and so detect aerosol scattering. Frost examined the performance of a variable phase function as an improvement to the constant phase function used previously. Mahony (1991) examined the effects of water vapor on aerosol optical depth retrieval. An estimate of water vapor content in a column of air can be derived by comparing the brightness temperature of two AVHRR windows in the thermal infrared region. He concludes that this effect can be compensated for, eliminating an error of 15% in the phase function.

The purpose of this study is to incorporate Mahony's improvement into the algorithm used by Frost, which did not account for water vapor appreciably affecting retrieved radiances. The April 1982 data examined by Frost will be re-evaluated to compensate for water vapor. The variable two-term Henyey-Greenstein phase function recommended by Frost will be examined in light of the new, water vapor corrected particle size phase function and compared to the values he generated.

B. MOTIVATION

Aerosols consist of a variety of solid or liquid material dispersed in the atmosphere; examples include volcanic ash, smoke, and pollen. These particles vary in their distribution and concentration in the atmosphere, which can impact local and global radiation budgets. The extreme concentrations of smoke particles resulting from the oil fires in

Kuwait created a layer that reduced daylight to night in the region. Even modest concentrations have demonstrated an impact in models of the earth's radiation budget (Weiss et al. 1974; and Coakley 1976). A Soviet study of longwave radiation in the tropical Atlantic ocean (Zaitseva 1976) linked short-term temporal changes in temperature to changes in aerosol particles.

Charlson et al. (1987) proposed that the major source of cloud condensation nuclei (CCN) over remote unpolluted oceans appears to be a waste product of phytoplankton, aqueous dimethylsulphide gas (DMS). A complex chain of chemical and biological processes result in DMS passing through the sea surface. Once in the atmosphere, it is oxidized to form sulfate aerosol particles which act as CCN. Varitions in phytoplankton populations with the associated changes in CCN particles could alter the earth's heat budget.

Of direct importance to the military is the impact of aerosols on electro-optical devices. The .4 to 1.0 μm waveband is considered the optimum window for lasers as it avoids ozone absorption at shorter wavelengths and water vapor absorption at longer wavelengths (Bloembergen et al. 1987). Aerosol scattering is a significant factor in this same waveband.

II. THEORY

A. DIFFUSE RADIANCE

Knowing that optical depths are small over the ocean and that single scattering is dominant (Pfeil 1986), and assuming an optically thin atmosphere, Frost (1988) used the following simplified version of the Radiation Transfer Equation (RTE):

$$L(\delta, \mu, \phi) \sim \left(\frac{\omega_0 F_0}{4\mu} \right) p(\Theta)\delta, \qquad 2.1$$

where,

L = diffuse radiance,

ϕ = azimuth angle,

ω_0 = single scatter albedo,

F_0 = solar irradiance,

μ = $\cos\theta$, (θ = satellite zenith angle),

p = scattering phase function,

Θ = single scatter angle,

δ = optical depth.

Griggs (1975) and Durkee et al (1986) demonstrated this linear dependence of radiance on optical depth.

There are three primary sources of satellite-detected radiance; aerosol scatter (L_A), Rayleigh scatter (L_R), and sea surface reflectance (L_S). This relationship can be expressed as

$$L = L_A + L_R + L_S \qquad 2.2$$

. Rayleigh scatter occurs when the size of the aerosol particle is much smaller than the wavelength of the incident radiation and, though strongly wavelength dependent, it does not vary spatially. Sea surface reflectance is very small for red wavelengths, the albedo is 0.5%, and zero for radiation with wavelengths longer than 0.7μm, except where the

sun-earth-satellite geometry results in sunglint (Ramsey 1968). Therefore, by avoiding data contaminated by sunglint, total radiance can be approximated by the sum of the radiances due to Rayleigh and aerosol scatter ($L \approx L_A + L_R$). By subtracting the component due to Rayleigh scatter, aerosol particle radiance (L_A) will remain:

$$L_A = L(\delta, \mu, \phi) - L_R \sim \left(\frac{\omega_0 F_0}{4\mu} \right) p(\Theta)\delta_A, \qquad 2.3$$

where δ_A is the aerosol particle optical depth.

With Rayleigh scatter forming a baseline radiance, aerosol scatter is the dominant source of upwelled radiance variations ($\Delta L \sim \Delta L_A$). Eqn 2.3 indicates satellite measured radiance is directly related to the changes in the aerosol particle characteristics of ω_0, $p(\Theta)$ and δ_A . It is apparent that a knowledge of p(Θ) variations is required to determine a more accurate δ_A from L_A.

B. OPTICAL DEPTH

Optical depth is a measure of the scattering and absorption material present in the atmosphere. It is determined by vertically integrating the extinction coefficient (σ_{ext}), from the earth's surface to the top of the atmosphere (H), expressed by

$$\delta = \int_0^H \sigma_{ext}\, dz. \qquad 2.4$$

Extinction is due to both absorption (σ_{abs}) and scattering (σ_{scat}) of radiant energy; however, in the marine environment, absorption can be neglected, leaving extinction due to scattering alone ($\sigma_{ext} \approx \sigma_{scat}$) such that

$$\delta = \int_0^H \sigma_{scat}\, dz. \qquad 2.5$$

The amount of scattering is determined by the size of the particles, their scattering efficiency, and the size distribution of particles in the column given by

$$\sigma_{scat} = \int_0^\infty \pi r^2 Q_{scat}(m, \lambda, r) n(r) dr, \qquad 2.6$$

where,

πr^2 = particle cross sectional area,

$Q_{scat}(m, \lambda, r)$ = scattering efficiency,

m = complex index of refraction,

λ = wavelength,

r = particle radius,

$n(r)$ = number distribution of particles.

Aerosol particles are most efficient in scattering radiant energy at wavelengths near their radius, becoming less efficient as the difference between the two increases. Any changes in the size distribution will produce a corresponding change in δ_A and in the observed radiance L_A. The variations in radiance between two wavelengths, specifically red and near-infrared, can be quantified by the ratio (Durkee et al. 1991)

$$S_{12} = \frac{(L_A)_{red}}{(L_A)_{nir}} \sim \frac{[\omega_0 P(\Theta)\delta_A]_{red}}{[\omega_0 P(\Theta)\delta_A]_{nir}} . \qquad 2.7$$

This ratio (S_{12}) is called the particle size index and is sensitive to variations in the slope of the particle size distribution, increasing as the slope increases. Small particles have the greatest influence if the slope is steep, while large particles are most important for more gradual slopes. Generally, $(L_A)_{red}$, due to small particle scattering, is greater than $(L_A)_{nir}$ resulting in an S_{12} ratio larger than 1 (Mahony 1991).

C. WATER VAPOR ABSORPTION

The dominant influence on retrieved radiances in the visible and near-infrared wavelengths is aerosol scattering. Though water vapor effects are not as significant as aerosol scatter, they can result in an over-estimation of S_{12} which could be interpreted as a change in aerosol characteristics or on the other hand, could mask a significant change. As the desired result is the estimation of aerosol particle characteristics from satellite observations, inclusion of water vapor effects will improve the accuracy of results.

In Figure 1, the effect of water vapor can be seen in the transmittance (τ) for AVHRR channels 1 and 2. Note that channel 1 τ is greater than channel 2, indicating less absorption is taking place. Therefore, L_2 would tend to decrease more due to absorption by water vapor than L_1 leading to the over estimation of S_{12}.

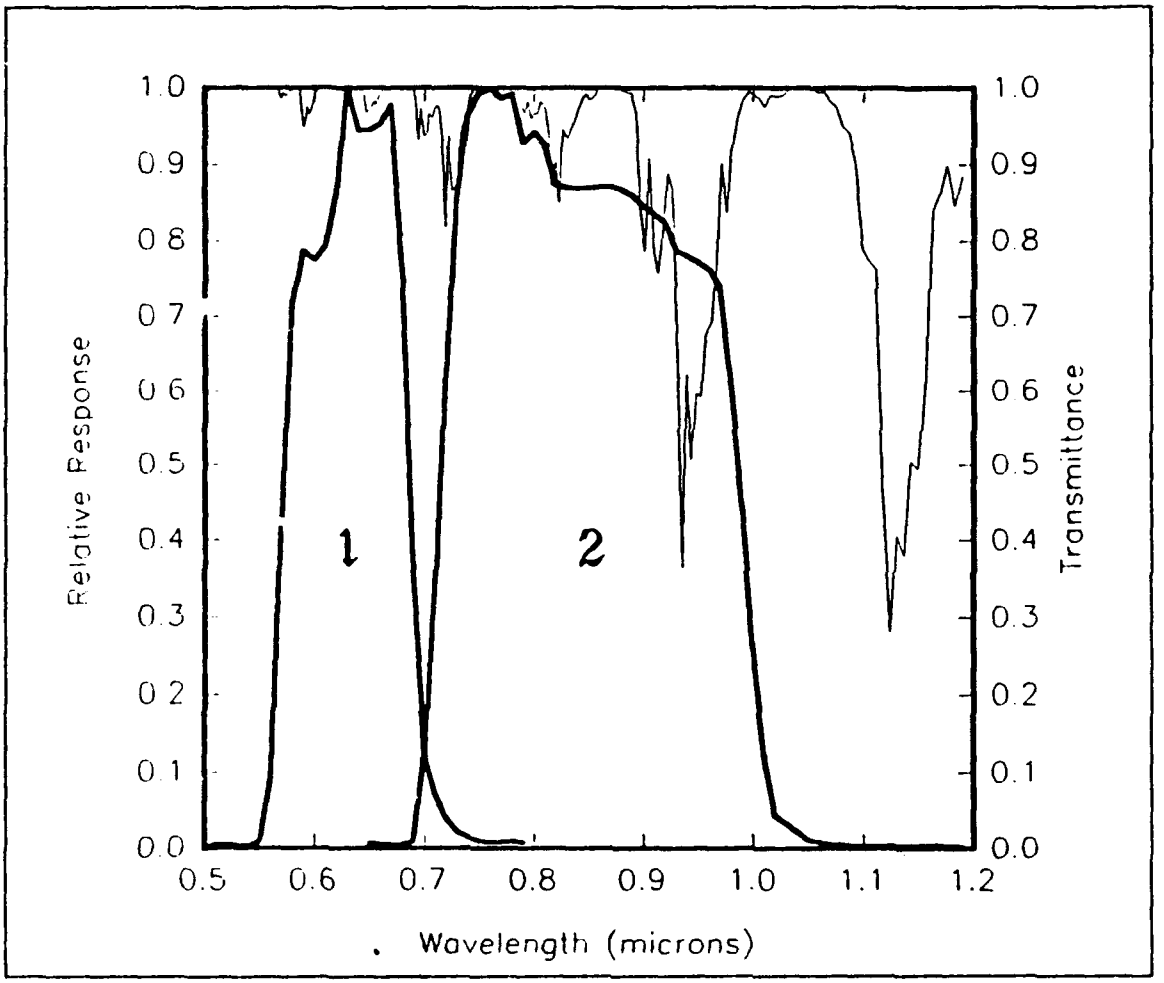

Figure 1. Atmospheric transmittance due to water vapor: Transmittance is shown with NOAA & AVHRR channels 1 and 2 response functions (Mahony 1991).

D. BRIGHTNESS TEMPERATURE DIFFERENCE

An estimate of the water vapor content in an air column can be made using the AVHRR 10 to 13 μm window region. In channels 4 and 5, at wavelengths of 11 and 12 μm respectively, absorption by water vapor is dominant while aerosol scattering is relatively insignificant. The benefits of using these channels is the colocation and temporal linkage with channels 1 and 2, providing a water vapor snapshot along the same path as the aerosol optical depth (δ_a) measurements. Although not the ideal sensor windows for water vapor content, their use is justified within the accuracy of the approximations made (Mahony 1991).

The brightness temperature (T) is determined from the radiance received, due to direct transfer, from the ocean surface to the satellite sensor. Therefore, the transmittance (τ) is directly proportional to the retrieved T. Only absorption reduces the radiance reaching the sensor; scattering is relatively insignificant.

Dalu et al. (1981) proposed a method for determining sea surface temperature using brightness temperature difference corrected for air column water vapor content. After manipulation of Dalu's formula, the vertically integrated water vapor density (w) is provided by

$$w = A(T_4 - T_5)\cos\theta. \qquad 2.8$$

where A is a constant. Using $A = 19600 g^{\circ} K^{-1} m^{-2}$, a scanning angle $\theta = 0$, and a variety of temperature and humidity profiles, Dalu (1986) applied this relationship to a radiative transfer model. The resulting line graph (Figure 2) has a correlation coefficient of $R = 0.99$, with an error of $\pm$ 1.5$kg\ m^{-2}$ in density.

Mahony determined that the water vapor influence on the particle size index was a function of w and $S_{12}(dry)$, the latter being the magnitude of S_{12} when $w = 0$. The equation for the curve that best fit his data is

$$S_{12}(dry) = \frac{S_{12}}{1 + 0.0332\sqrt{w}}, \qquad 2.9$$

where S_{12} and w are determined from measured radiances.

E. VARIABLE PHASE FUNCTION

Based on Frost's work, a variable single scatter phase function was used, having been determined to be more accurate in its optical depth estimation. Higher ratios, which are due to smaller particles, have more backscatter than the lower ratios, due to larger particles. This provides the basic shape necessary for the phase function needed to estimate optical depth.

The two-term Henyey-Greenstein scattering phase function (Lenoble 1985) was used.

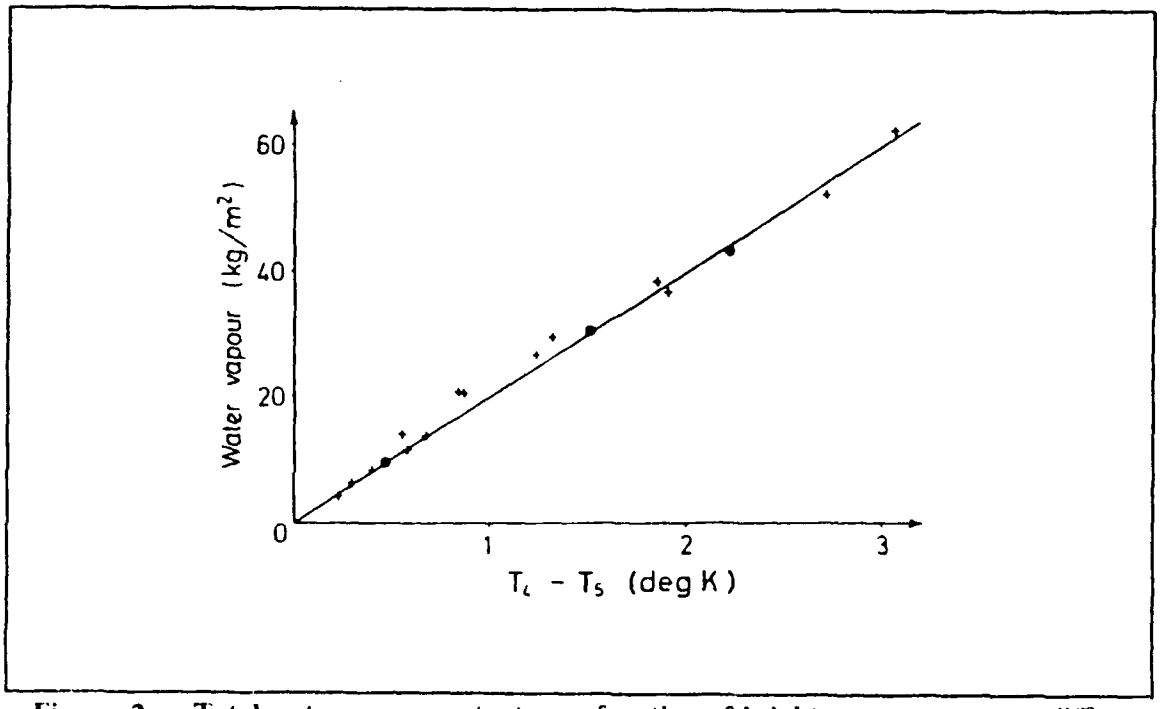

Figure 2. Total water vapor content as a function of brightness temperature difference (Dalu 1986).

$$p(\Theta) = \frac{W'(1-g_1^2)}{(1+g_1^2-2g_1\cos\theta)} + \frac{(1-W')(1-g_2^2)}{(1+g_2^2+g_2\cos\theta)}, \qquad 2.10$$

where W' is a weighting factor, g_1 and g_2 are asymmetry curve factors, and θ is the scatter angle. All three of these factors are functions of S_{12} written as

$$W' = 1.2 - (0.25 \times S_{12}), \qquad 2.11$$

$$g_1 = 1.04 - (0.08333 \times S_{12}), \qquad 2.12$$

$$g_2 = 1.2 - (0.58333 \times S_{12}). \qquad 2.13$$

From the equations 2.11 through 2.13, the phase function's dependence on S_{12} is apparent. The marine-type phase function describes large particle distribution, low S_{12} ratios; while the rural-type phase function follows small particle distribution, high S_{12} ratios.

As the ratios change, the factors change, resulting in a varying phase fuction from one similar to a marine phase function to one similar to a rural phase function. Figure 3 shows some of the variable phase functions $p(\Theta)$ calculated by Frost (1988) from the indicated S_{12} values.

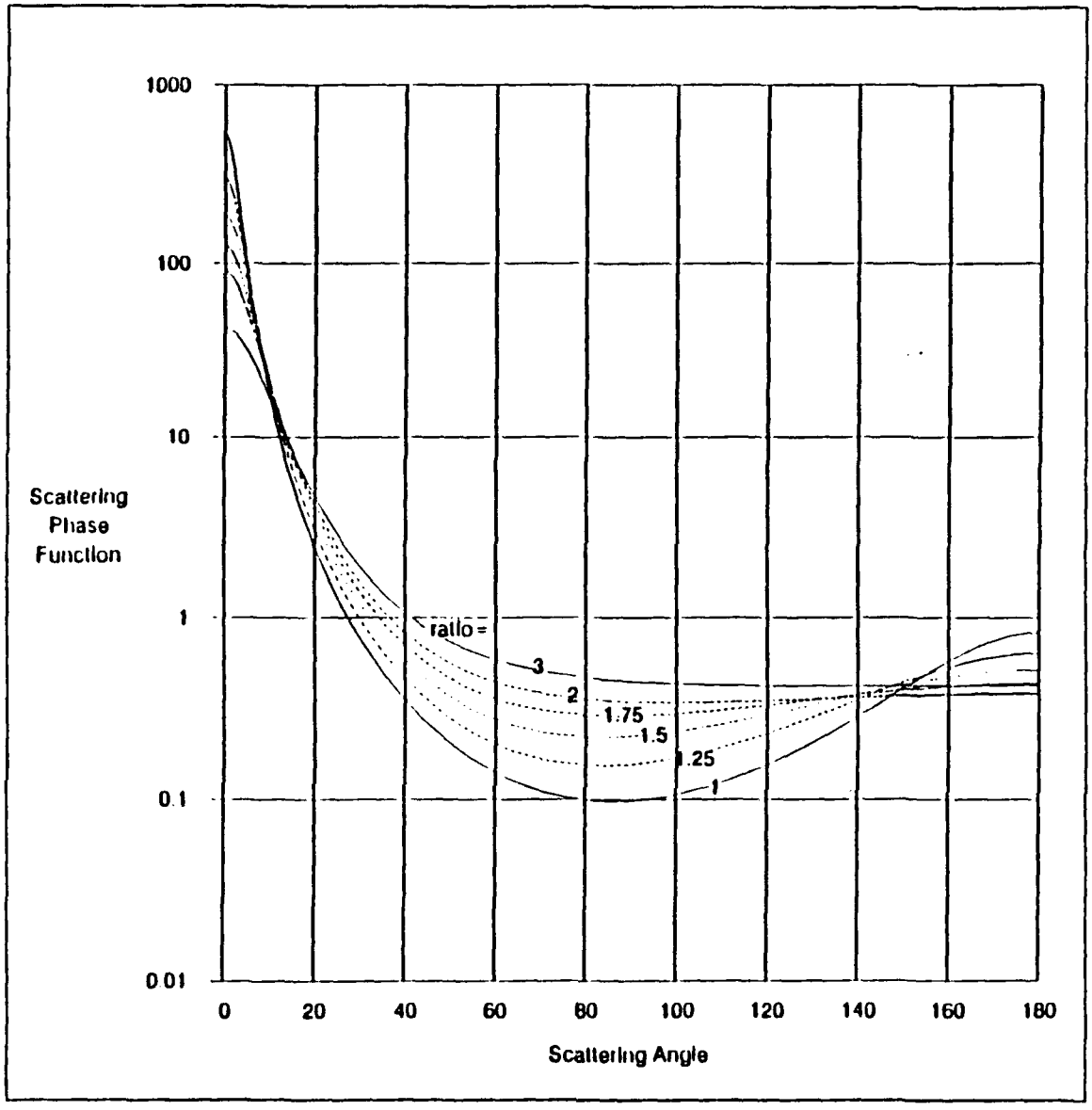

Figure 3. Aerosol particle size index and associated phase functions: (Frost 1988).

III. PROCEDURES

A. DATA AND PROCESSING

The data examined was collected by the NOAA 7 polar orbiting satellite whose average altitude was 833 km. This sun-synchronous platform crossed the equator at approximately 0230 and 1430 local standard time (north- and south-bound, respectively). Of the five spectral bands or channels on the AVHRR instrument; channels 1, 2, 4, and 5 were used in measuring upwelling radiance. Table 1 provides the bandwidths for all the channels (Jensen 1986) plus a weighted average of the solar irradiance (F_0) over the bandwidth used for channels 1 and 2 calculations.

Table 1. NOAA 7 AVHRR CHANNEL BANDWIDTHS.

Channel	*Bandwidth*	*Solar Irradiance*
1	0.58-0.68 μm	154.3536 $mWcm^{-2}$
2	0.725-1.10 μm	103.0908 $mWcm^{-2}$
3	3.55-3.93 μm	
4	10.5-11.3 μm	
5	11.5-12.5 μm	

The archives of the National Center for Atmospheric Research (NCAR) in Boulder, Colorado, provided AVHRR Global Area Coverage (GAC) data for two periods in April 1982; the 5th - 10th and the 20th - 25th. April 1982 data was analyzed for comparison with the work done earlier by Frost (1988).

All the data was processed on the Interactive Environmental Digital Analysis Laboratory (IDEA LAB) located at the Naval Postgraduate School, Monterey, CA. The IDEA LAB produced enhanced images and graphs from the processed data.

B. ANALYSIS

The data analysis scheme was based on that used by Pfiel (1986) and Frost (1988). The water vapor algorithm used by Dalu (1986) was incorporated to account for absorption by water vapor, as recommended by Mahony (1991). Also accounted for in the algorithm were changes to the solar irradiance due to variations in the sun-earth distance. During preprocessing, pixels located at latitudes greater than 70° or those over land were discarded.

To remove sunglint, an empirical method using viewing geometry was applied. This method, a weighted sum of relative zenith and azimuth angles for the sun and satellite, identified approximately the same contaminated areas as the Avian sunglint routine, which is based on the Cox and Munk (1954) method.

Ozone absorption effects occur in the red and near infrared wavelengths with the greatest absorption at a wavelength of 0.69μm (Fleagle and Businger, 1980), which is in the channel 1 window. This effect was inadvertently compensated for twice by Frost. The error has been corrected for this study.

Each pixel was then examined for clouds as only clear pixels were to be processed. Cloud removal was performed by the same method used by Frost:

1. Test for bad pixels -- If channel 2 or channel 4 radiance values are less than zero, after Rayleigh radiance was removed, then the pixel is classified as "bad" and not processed.
2. Test for high clouds -- A pixel was considered to contain high clouds if its channel 4 brightness temperature was less than 273°K.
3. Test for low clouds -- A pixel was considered to contain low clouds if its channel 2 albedo was greater than 40%.
4. Preliminary test for clear pixels -- A channel 1/channel 2 albedo was calculated and if that ratio was greater than 1.5, the pixel was tentatively classified as clear.
5. Final test for clear pixel -- The channel 2 albedo of the pixel tentatively identified as clear was compared with the four pixels above, below, to the right and to the left. All the pixels must fall with in five counts of each other for the pixel to be classified as clear, otherwise it was counted as partly cloudy. A count is equivalent to 0.1069% albedo (Kidwell 1986).

The clear pixels were then processed for a variety of parameters. The list is basically the same as Frost's, the most significant difference is the inclusion of two parameters with the water vapor correction, the terms include the word "dry" in their name.

Channel 1/Channel 2 ratio,

Dry Channel 1/Channel 2 ratio,

Aerosol optical depth,

Dry Aerosol optical depth,

Average phase function of Channels 1 and 2,

Channel 4/Channel 5 brightness temperature differences,

Number of clear pixels,

Number of partially cloudy pixels,

P parameter.

The P parameter is used to examine the phase function calulated by Frost.

The phase function $p(\theta, S_{12})$ is an important factor in the determination of aerosol optical depth. Any changes made in the phase function algorithm, such as the addition of a water vapor correction to S_{12}, will produce corresponding changes to the calculated optical depths. A comparison of this modified phase function to that determined by Frost should provide confirmation that the changes made produce physically sound results and add to the knowledge of $p(\theta, S_{12})$.

A new parameter was defined using the simplified RTE (2.1) that is calculated from radiance data and can be used to derive $p(\theta)$ and δ_A:

$$P \equiv \frac{4\mu L_A}{F_0} \approx p(\theta, S_{12})\delta_A. \tag{3.1}$$

Using the fact that integrating the phase function over a sphere is unity, the following form can be used to determine $p(\theta, S_{12})$:

$$\int p(\theta, S_{12})d\Omega = \int Ap(\theta, S_{12})\delta_A d\Omega = \int AP d\Omega = 1, \tag{3.2}$$

where A is equal to the inverse of the optical depth. It is this equation from which the phase function will be calculated for comparison to Frost's curves.

All of the results were stored and averaged in 1° by 1° boxes; each data point is one box. The number of pixels varied from box to box, depending on the number of partially cloudy to cloudy pixels found in each square.

IV. RESULTS

A. INTRODUCTION

Ongoing efforts to determine aerosol particle characteristics have resulted in a steady improvement in the algorithm. Water vapor effects were shown to be an important factor in aerosol optical depth retrieval but have not been previously applied to satellite data. In this study the latitudinal variation in water vapor content is initially examined to give an overview of where the effects could be the most significant. Particle distribution characteristics are examined next, both with and without the water vapor correction. The data having the correction will be refered to as "dry". Both the corrected and uncorrected particle size index and aerosol optical depth will be examined and compared over the Pacific Ocean followed by the latitude profiles of the averaged values. Finally, the shape of the P parameter curves are compared to Frost's phase function curves.

B. COLUMN WATER VAPOR

Figures 4 and 5 show the average water vapor content in an air column to provide a general overview of water vapor effects in the atmosphere for the periods of April 5 - 10 and 20 - 25, respectively. The general structure is that of a maximum in the vicinity of the equator with values then decreasing toward the poles.The drop is more rapid in the northern hemisphere than the southern hemisphere, the latter is transitioning from its summer season when temperatures are higher and more water vapor is present. The greater year-round air and sea surface temperatures at the equator allow more water vapor to exist in a column of air. From this it can be seen that the greatest potential for error due to water vapor is in the equatorial region. An examination of the particle size index before and after applying the water vapor correction will be made next.

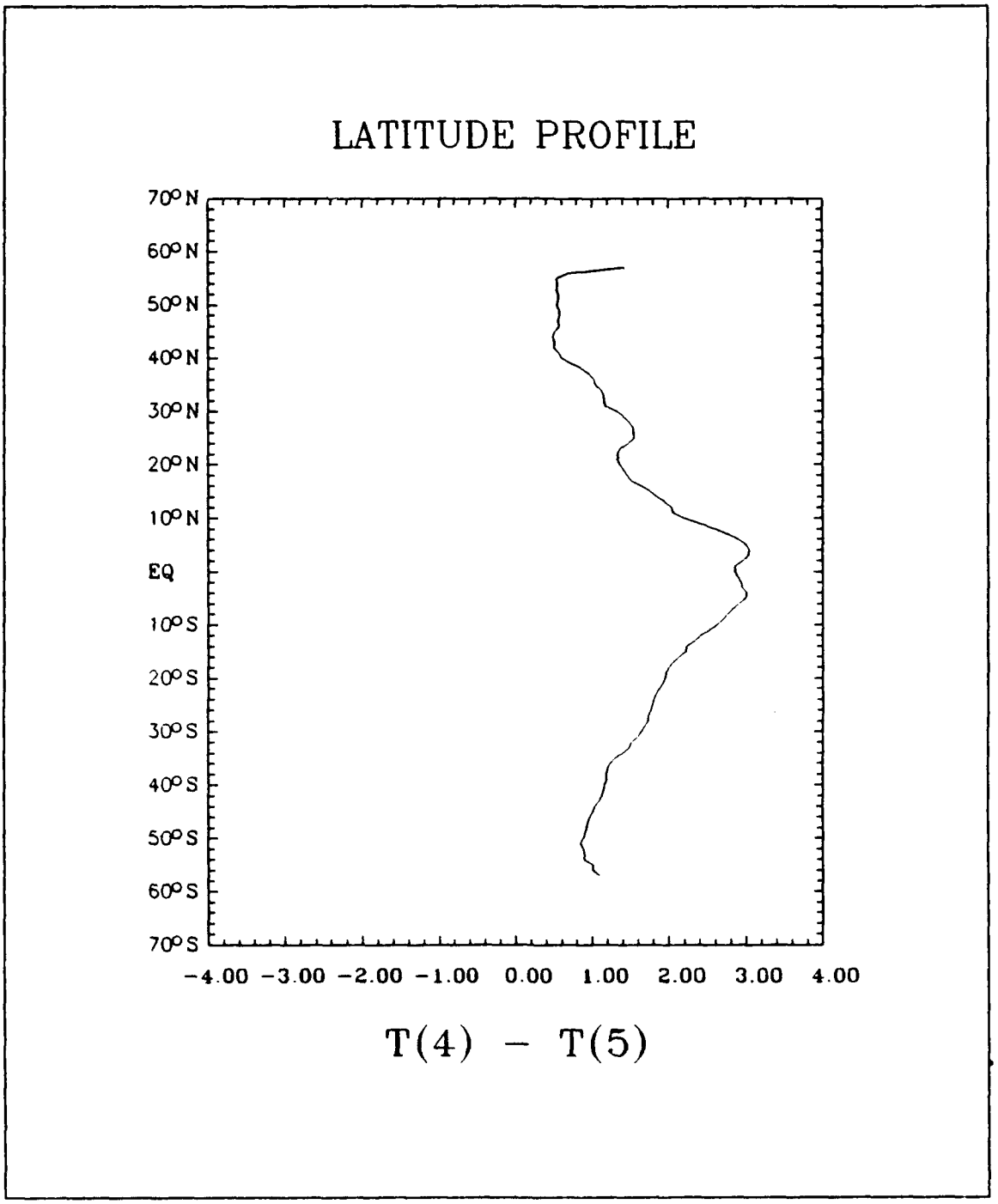

Figure 4. Brightness temperature difference for April 5 - 10.

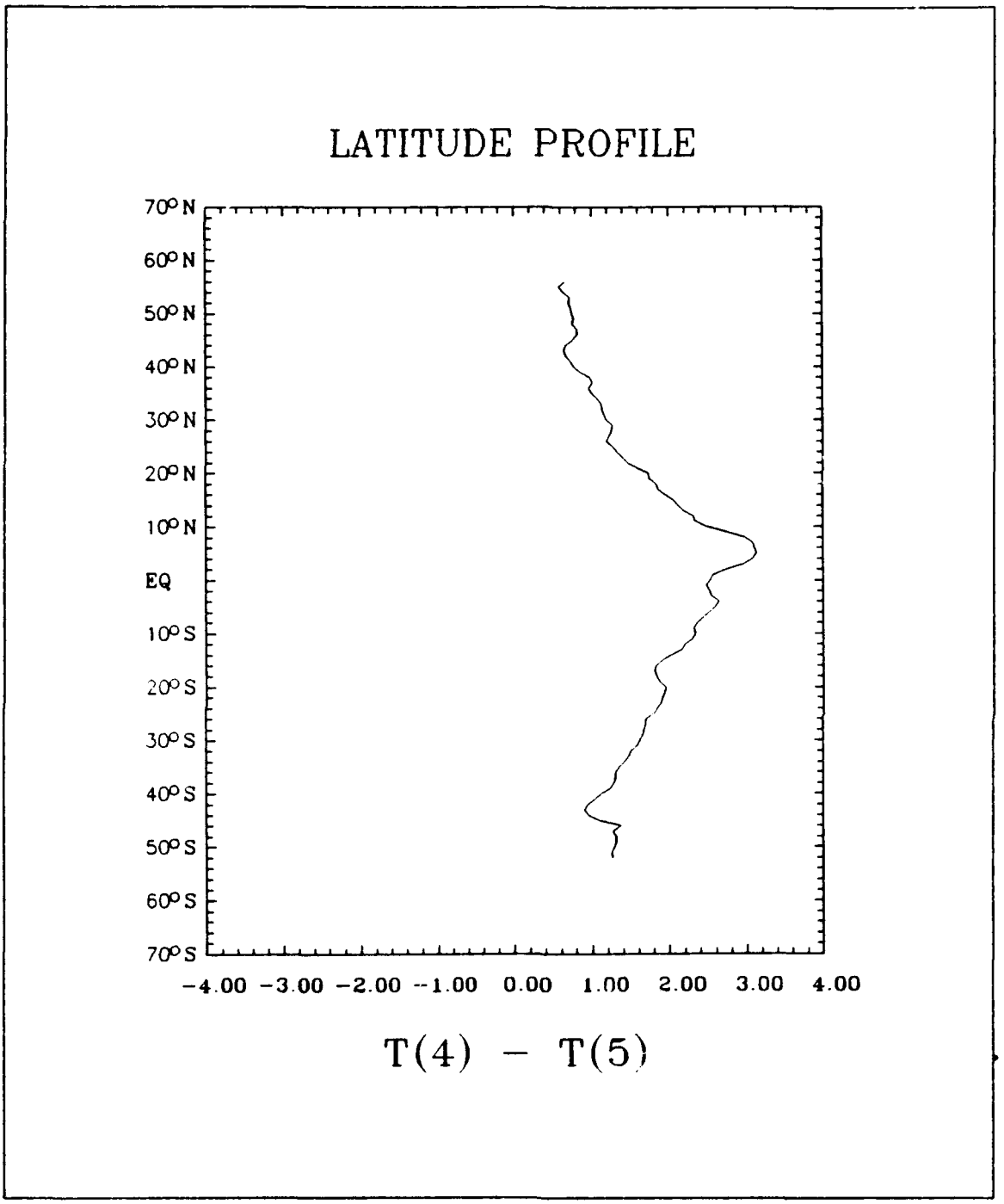

Figure 5. Brightness temperature difference for April 20 - 25.

C. PARTICLE SIZE INDEX

Figures 6 and 7 depict the uncorrected S_{12} values across the Pacific Ocean for April 5 - 10 and 20 - 25, respectively. A broad region of high values extends across the low latitudes in the southern hemisphere in both figures, indicating the presense of a greater number of smaller particles. Low values indicating larger particles can be seen in Figure 6 across the northern hemisphere. In Figure 7 there are two noticable maxima; one in the vicinity of the New Hebrides islands, the second west of South America. The north Atlantic appears to be a region of small particles except along the east coast of the United States.

In Figures 6 and 7, bands cross each figure from north-northwest to south-southeast. These are a result of the moving of the sensor's aperature to the left and right of the satellite's path to view the side regions. Aerosol scatter is anisotropic, favoring forward and backward scatter. A satellite is looking at backscatter when it looks directly at the earth. But as the sensor looks to the side, it is no longer viewing backscatter, but the smaller scatter associated with smaller scattering angles. This results in a decrease in the phase function and a corresponding increase in the optical depth. Future work will need to correct for this effect.

Figures 8 and 9 show a comparison of the particle size index profiles for S_{12} and $S_{12}(dry)$ for early and late April, respectively. The S_{12} profiles in both figures show a broad region of high values, approximately 2.35, from the equator to 40°S; the values then decrease toward the poles more rapidly in the southern hemisphere than in the northern. The greatest drop can be seen in the southern hemisphere in Figure 8 with a minimum value of 2.0. The minimum in Figure 9 is 2.10. Frost's values were 2.0 at the equator decreasing to 1.65 moving southward toward the pole; a second smaller decrease occurred toward the north pole, dropping to 1.9. His underestimation was due to a

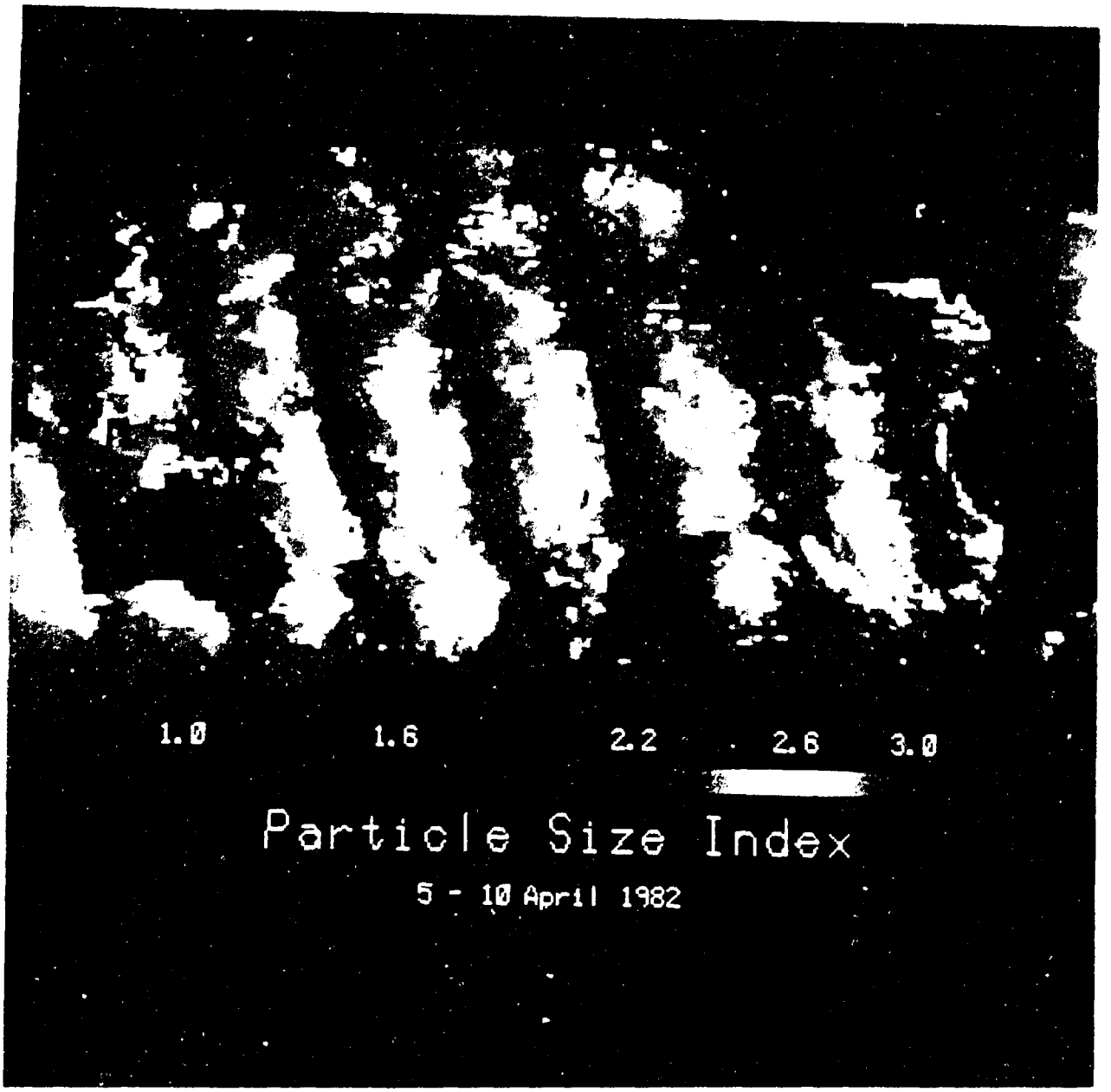

Figure 6. Particle size index over the Pacific, April 5 - 10

Figure 7 Particle size index over the Pacific, April 20 - 25

D DRY PARTICLE SIZE INDEX

Figures 10 and 11 depict the $N_{1.0}/N_{3.0}$ values across the Pacific Ocean. A comparison of the uncorrected $N_{1.0}$ values in Figures 6 and 7 show that the particle size index values decreased significantly after the correction was applied. Open ocean regions are now uniform with no significant difference between hemispheres.

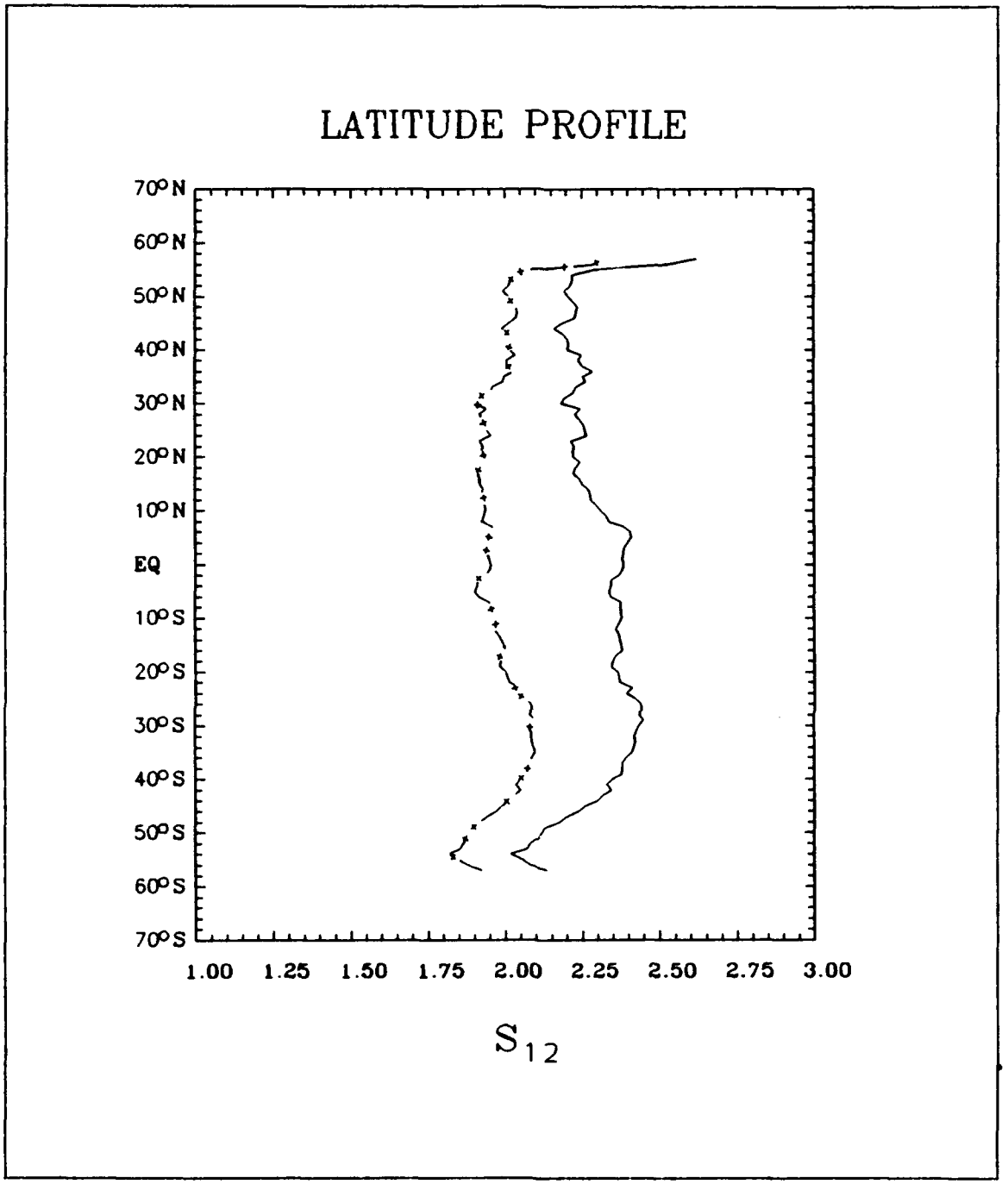

Figure 8. Comparison of particle size index profiles for April 5 - 10: the solid line is S_{12}, and the dashed line is $S_{12}(dry)$.

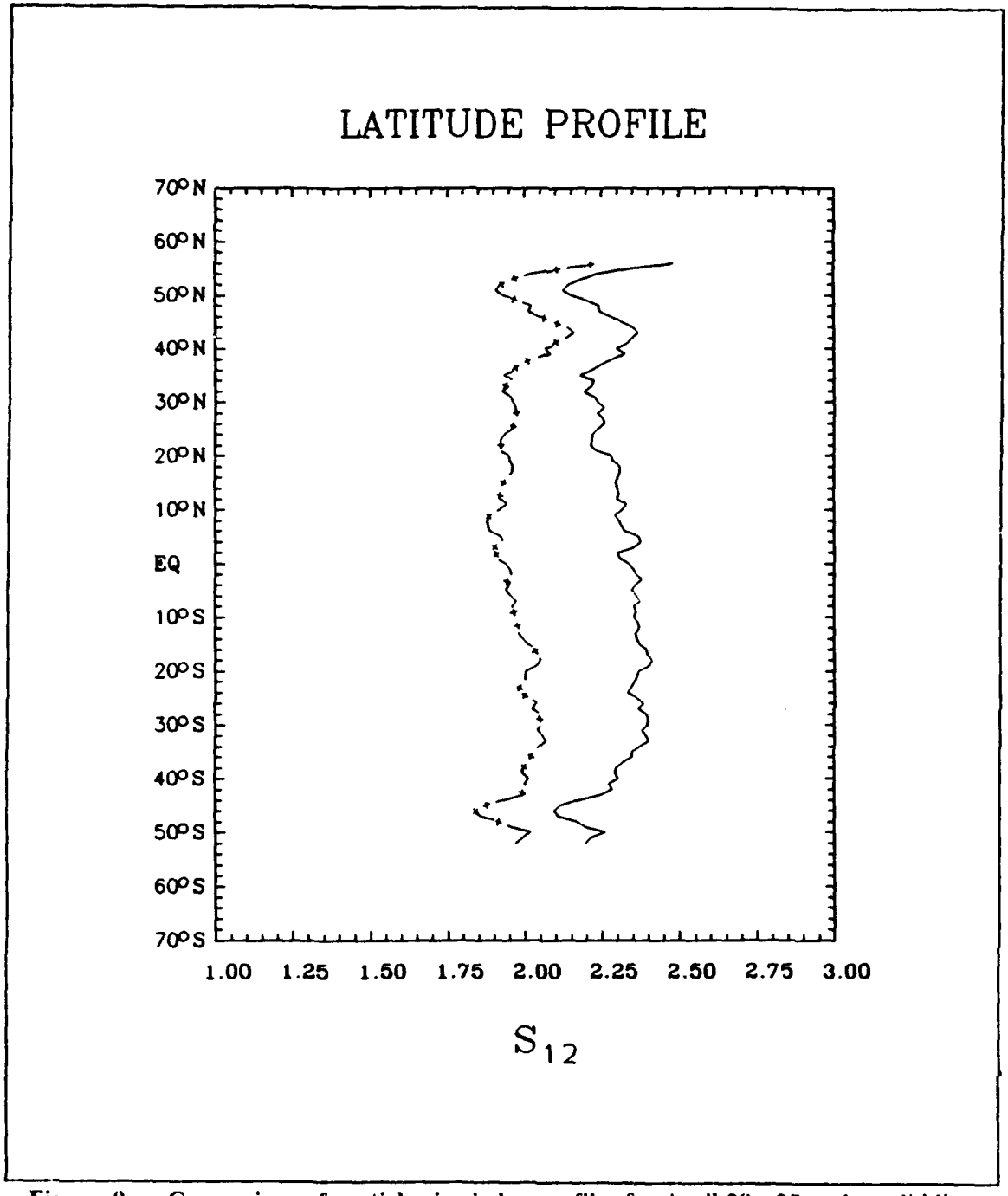

Figure 9. Comparison of particle size index profiles for April 20 - 25: the solid line is S_{12}, and the dashed line is $S_{12}(dry)$.

In early April, Figure 10, distinct high value areas remain in the Gulf of Carpentaria and along the coast of China. Late April (Figure 11) shows two areas of higher values in the northern Atlantic Ocean and along the west coast of North America. The maximum west of South America in Figure 7 is easier to distinguish in Figure 11 and has lower values. The maxima off the Americas appear to be associated with upwelling regions that are biologically very productive, which could be a source for the greater number of small aerosol particles.

In Figures 8 and 9, it is easy to see the decrease in size index values between S_{12} and $S_{12}(dry)$. At the equator $S_{12}(dry)$ is 0.5 less than S_{12} in early April, 0.4 less later in the month. From the equator to the poles, the difference between S_{12} and $S_{12}(dry)$ decreases to approximately half the values at the equator in both figures. In both instances the overall shape of the $S_{12}(dry)$ curve shows a minimum near the equator gradually increasing as you move toward the poles, which is the reverse of Frost's results where values decreased toward the poles. Though a more uniform profile was expected, the peaks that exist in the corrected profiles of both figures correspond to the latitudes of the maxima depicted in Figures 10 and 11.

E. OPTICAL DEPTH

The views of the Pacific in Figures 12 and 13, show the southern hemisphere with low optical depths and the northern hemisphere with very high optical depths. The largest feature is the wide area of high values, 0.45 to 0.50, that occurs along the Mexican Central American west coast extending westward into the Pacific. This feature is the result of the El Chicon volcano (17.3°N, 95.2°W) erupting on a number of occasions during the period of 28 March to 6 April. The high values in the Gulf of Mexico are also the result of El Chicon. The movement to the east is possibly due to stratospheric winds carrying particles ejected to those heights (Frost 1988). In early

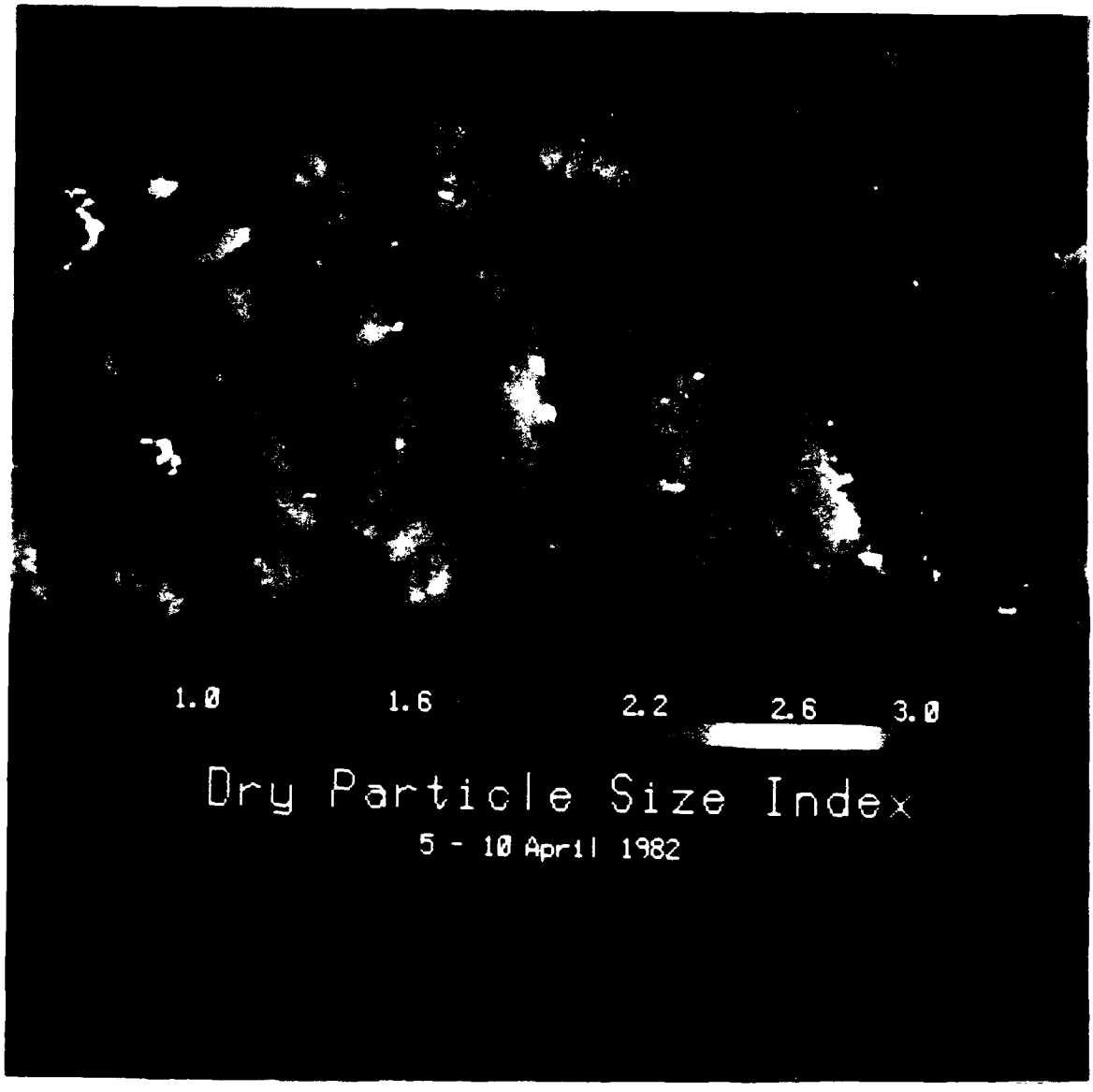
1.0
1.6
2.2
2.6
3.0
Dry Particle Size Index
5 - 10 April 1982

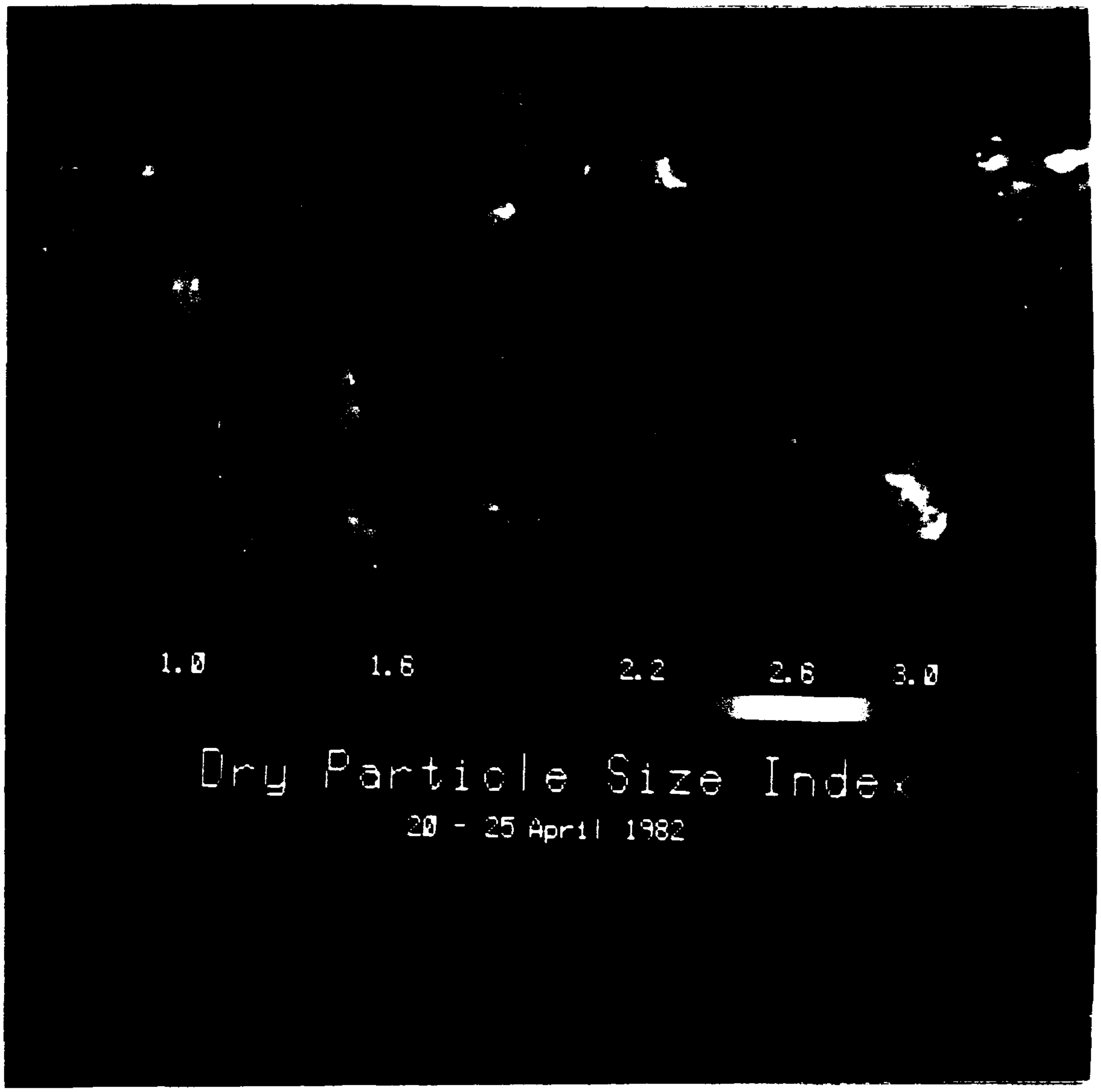

Figure [illegible]. Dry particle size index over the Pacific, April 20 – 25.

[illegible] een the optical depth profiles for [illegible] and [illegible] shows [illegible] value of 0.2 at approximately 20°N [illegible]. A second peak located [illegible]. The reason for the maximum is [illegible] Antarct[illegible]

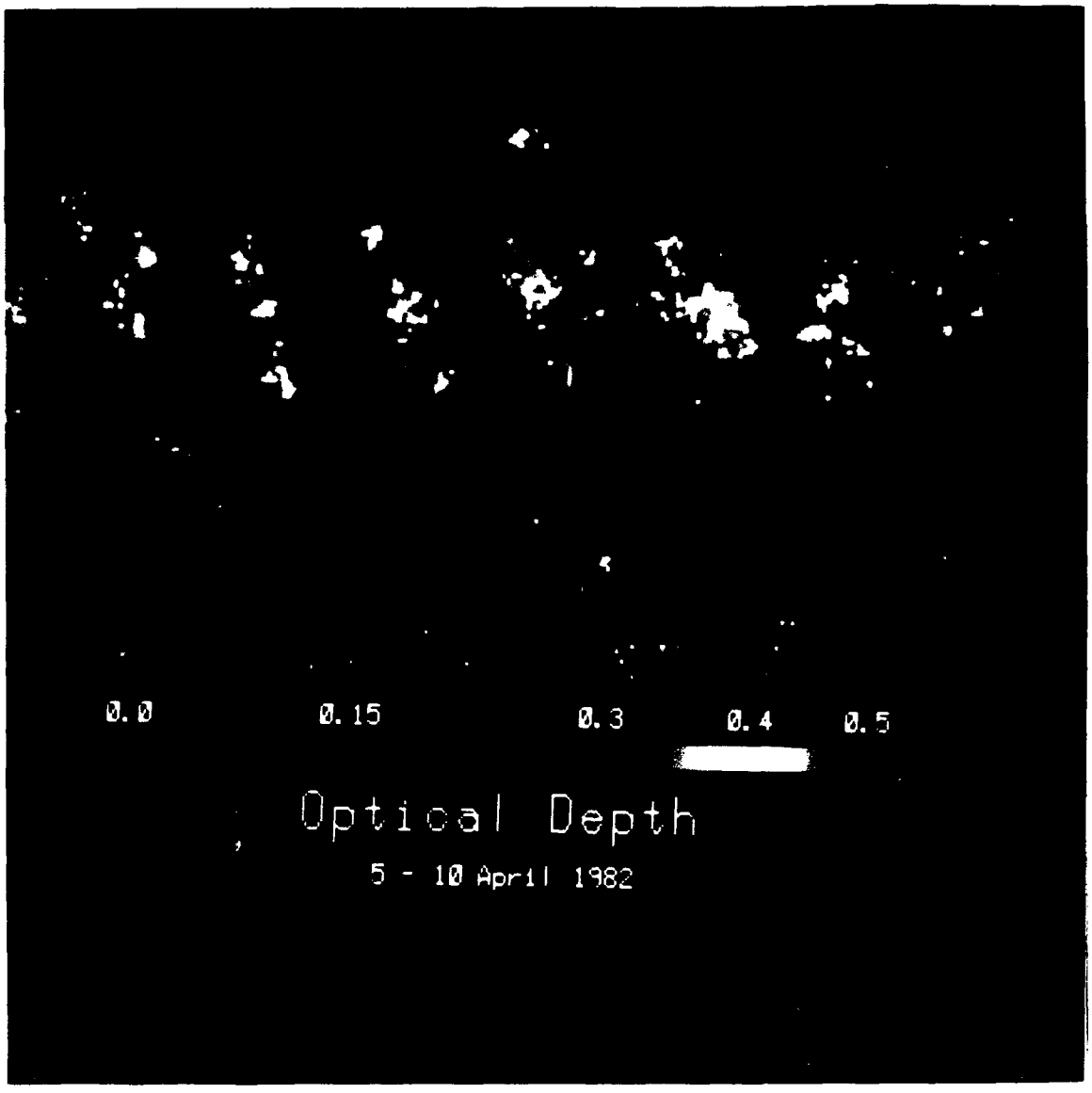
0.0
0.15
0.3
0.4
0.5
Optical Depth
5 - 10 April 1982

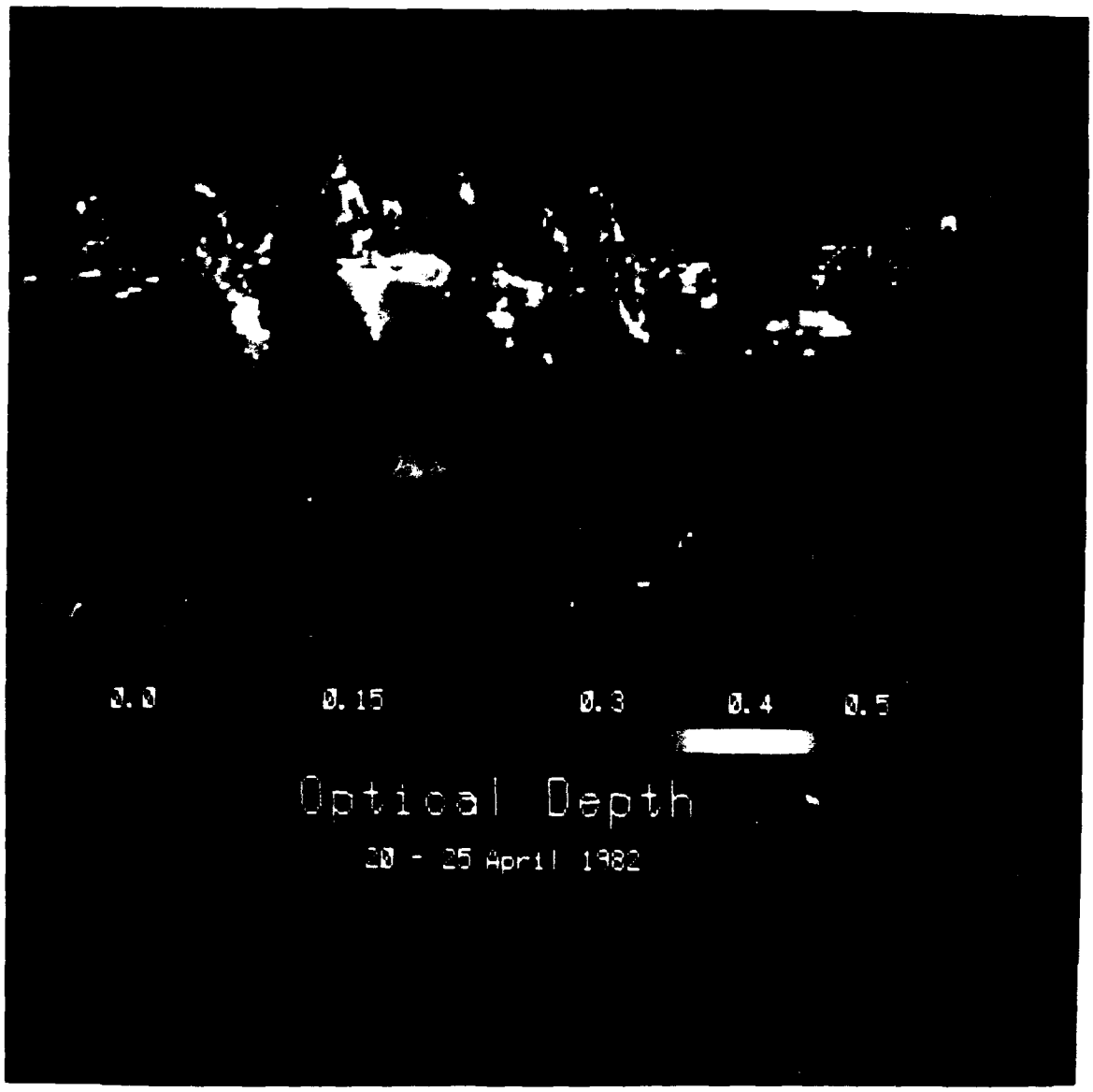

Figure 13. Optical depth over the Pacific for April 20 - 25.

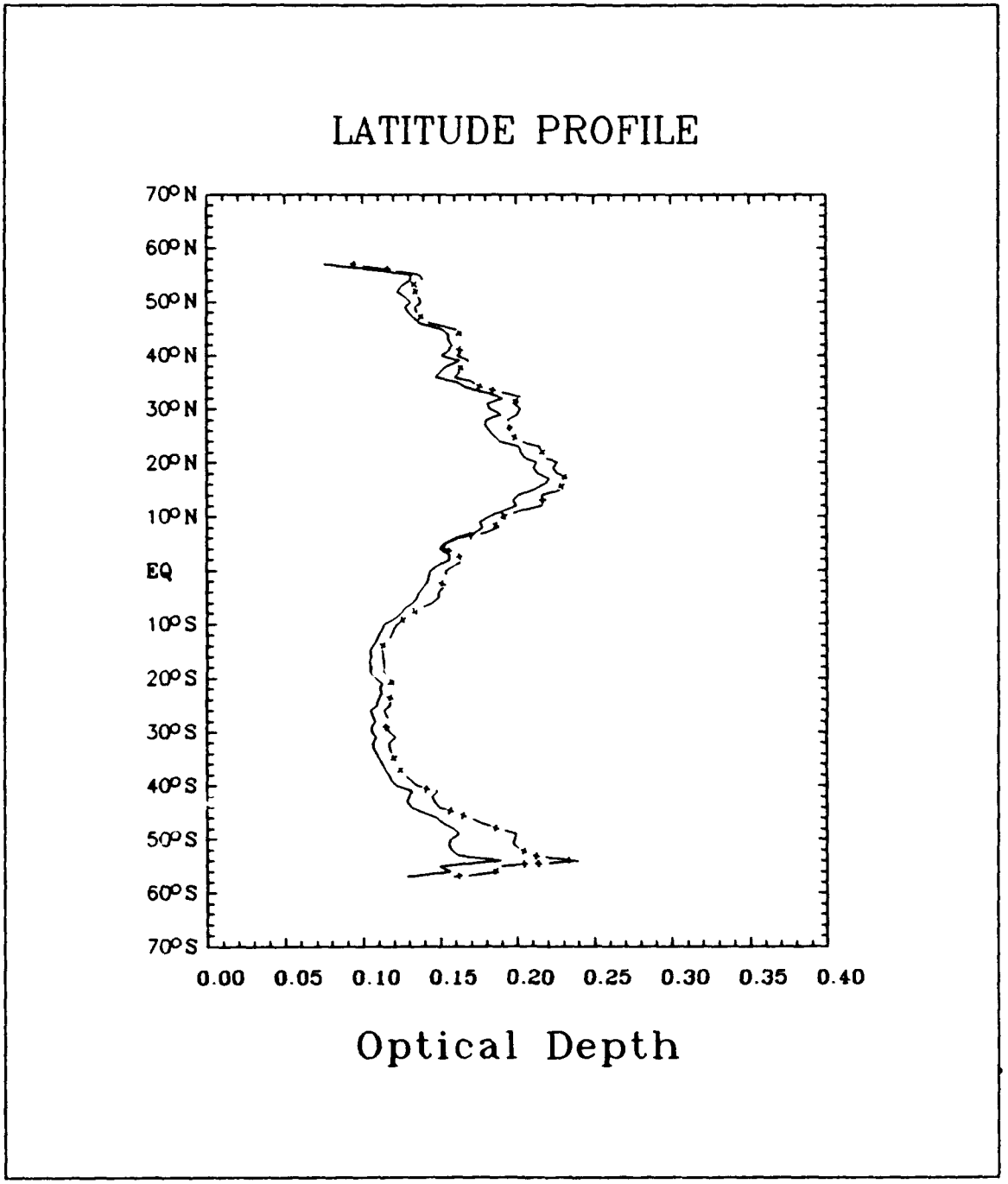

Figure 14. Comparison of optical depth values for April 5 - 10: solid lines are δ_A values, dashed are $\delta_A(dry)$ values.

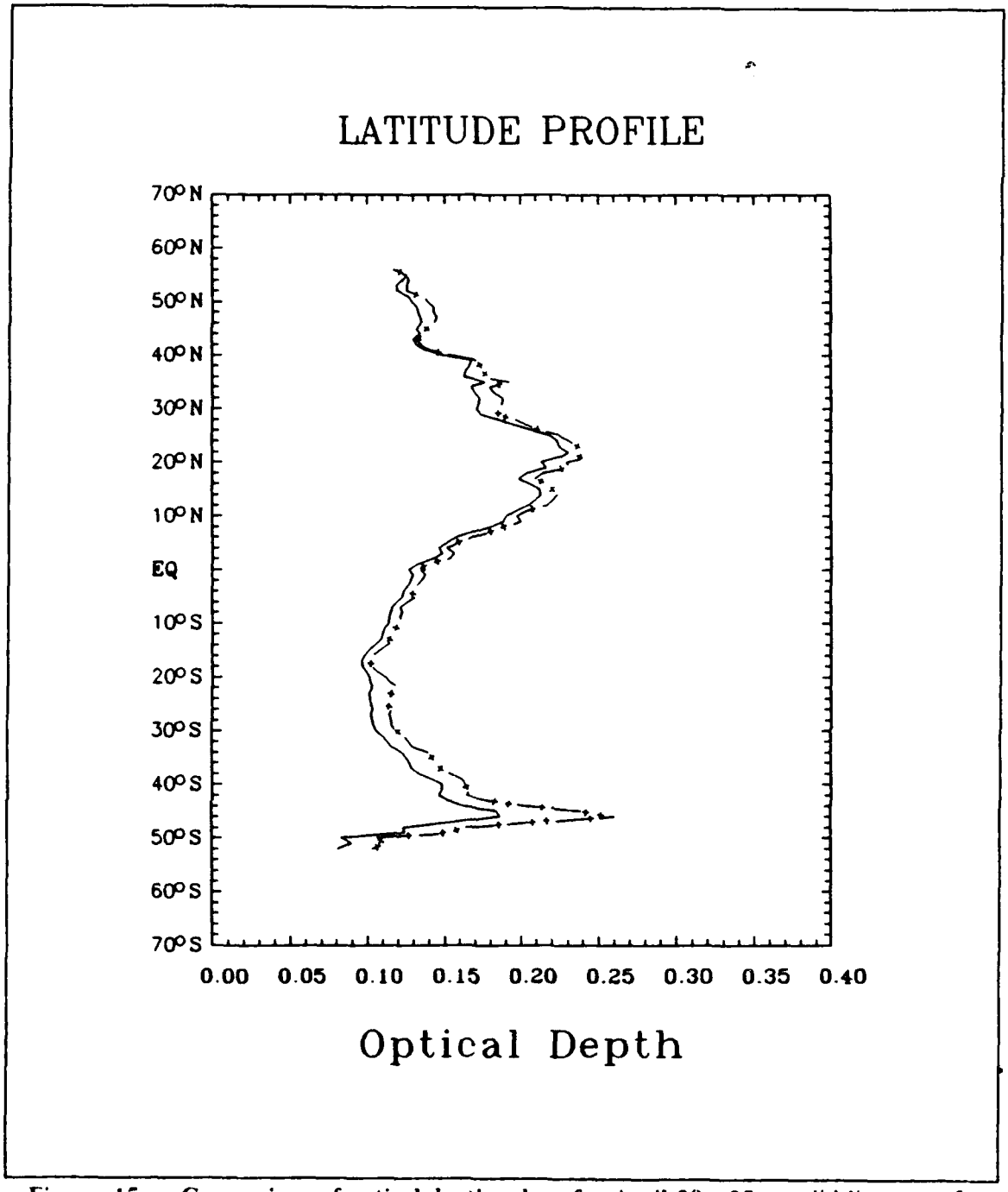

Figure 15. Comparison of optical depth values for April 20 - 25: solid lines are δ_A values, dashed are $\delta_A(dry)$ values.

changes occur in areas where the number of aerosol particles are sufficient to affect the optical depth.

G. PHASE FUNCTION

Figure 18 shows the P parameter as a function of scatter angle for three different particle size indices. A comparison to Frost's plot of the Henyey-Greenstein phase function (figure 3) indicates that the basic shape of the P parameter curves are similar to that shown by Frost. A smaller particle size index has a larger value in the forward direction (between 0° and 60°) than larger index values. The larger the particle size index the closer the curve approaches that of Rayleigh scatter, which is expected as smaller particles dominate. Where the scatter angle is between 90° to 140°, the P parameter approaches a minimum value for each curve. As the angle increases to 180° the curves show an increase in P values.

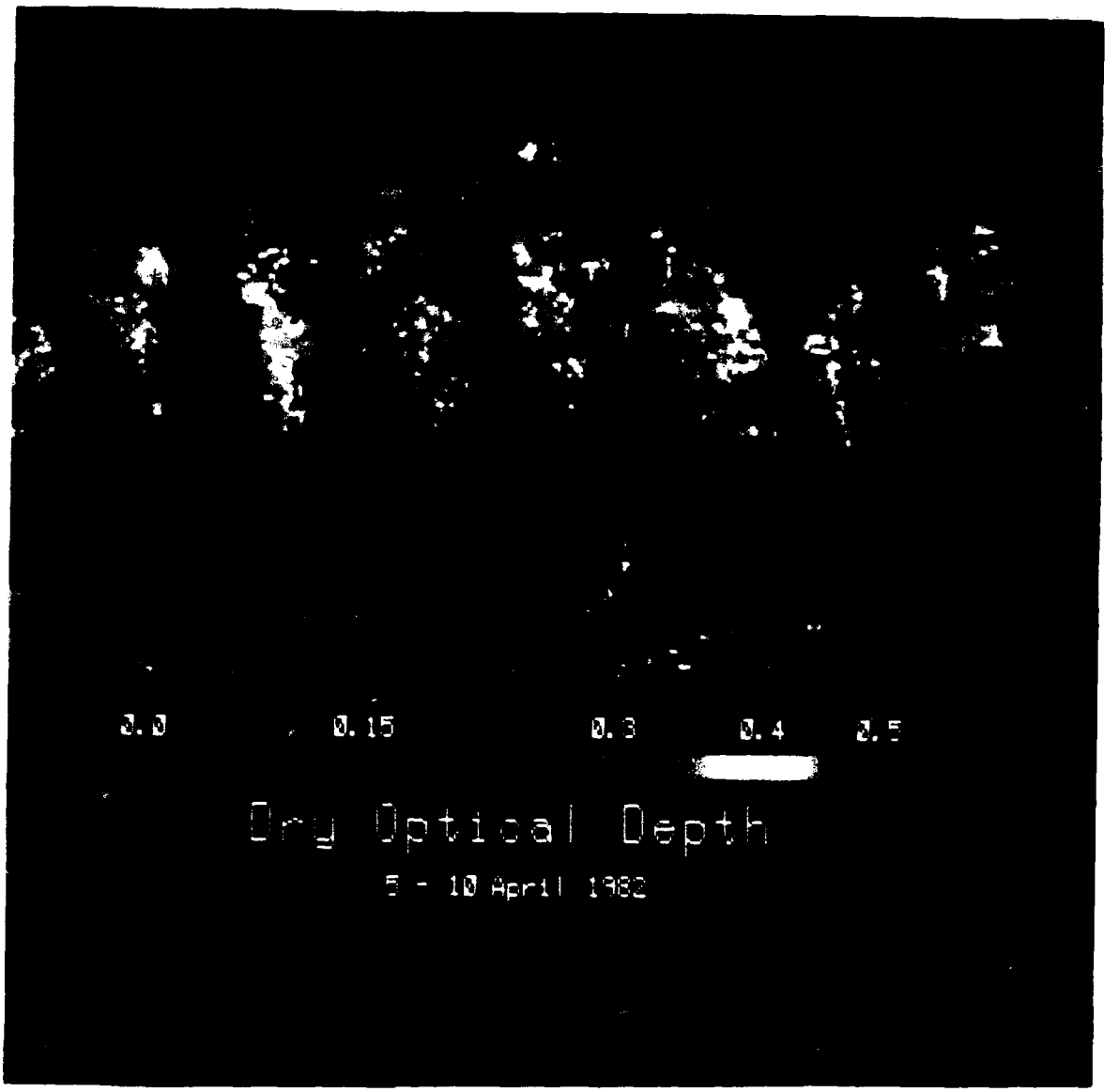

Figure 4a. Dry optical depths over the Pacific basin, April 5 - 10.

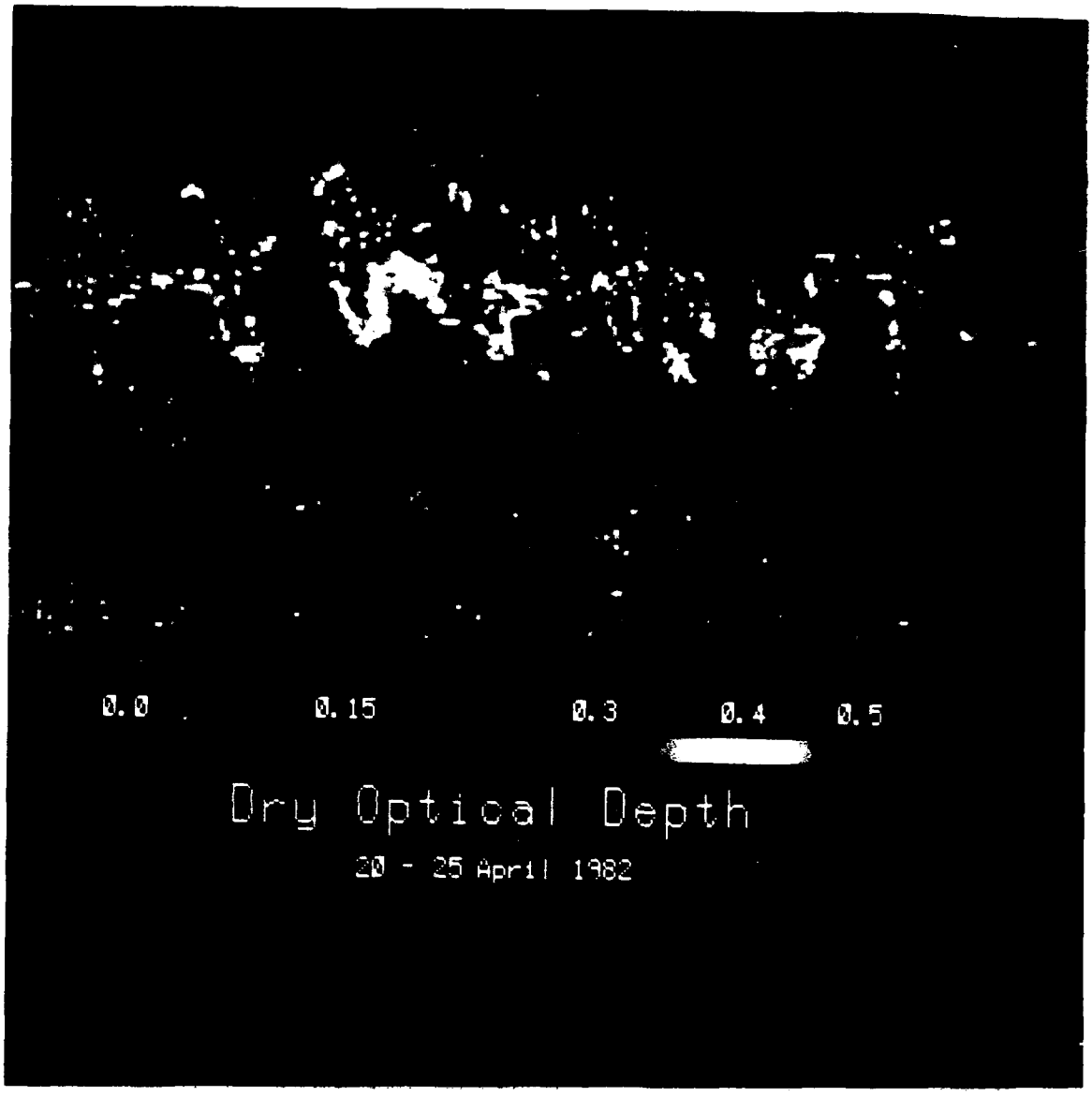

Figure [illegible] Dry optical depths over the Pacific basin, April 20 - 25.

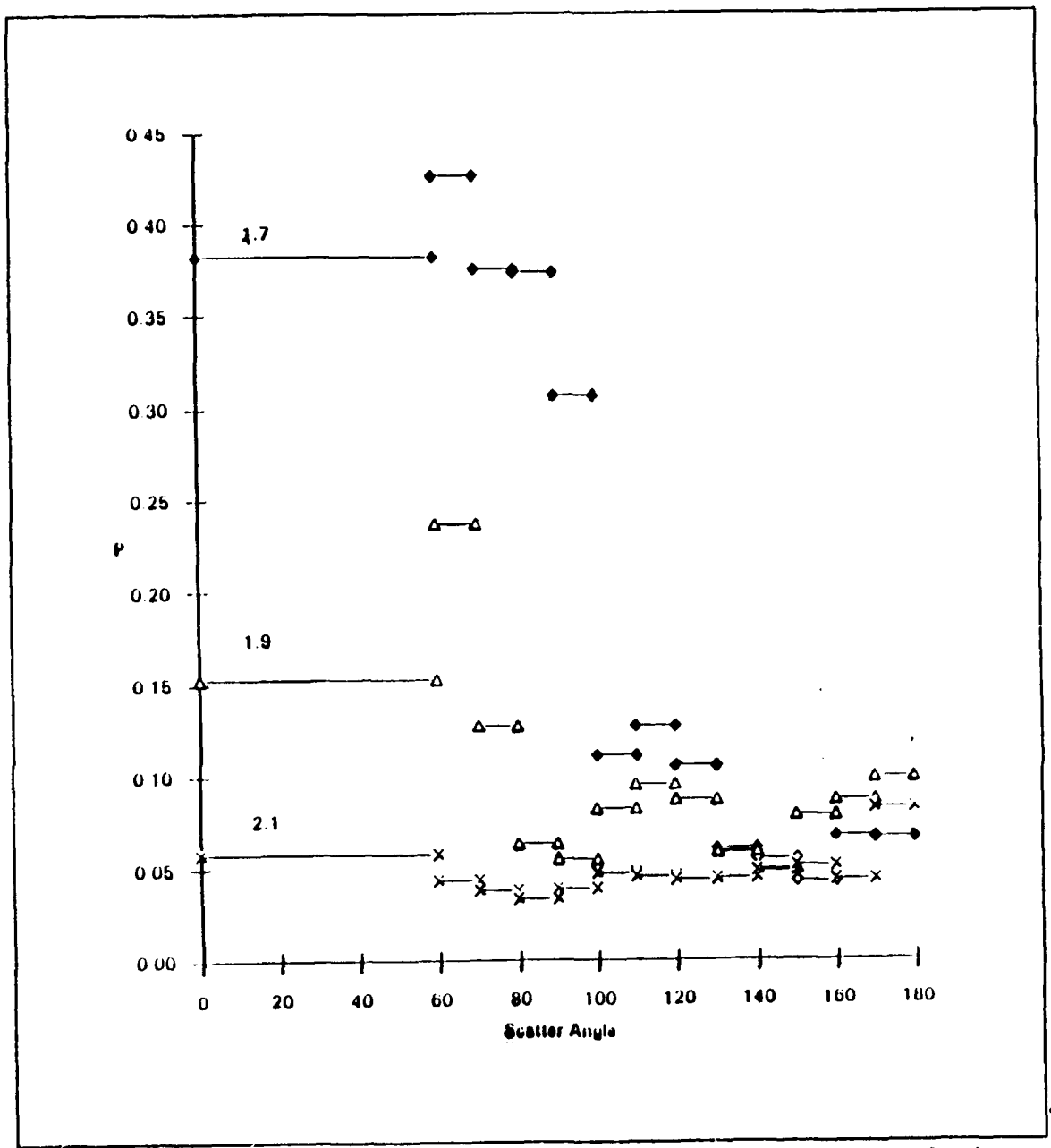

Figure 18. P parameter as a function of scatter angle: Values are shown for three particle size indices; 1.7 (diamonds), 1.9 (triangles), and 2.1 (x's).

V. CONCLUSIONS AND RECOMMENDATIONS

Frost showed that his technique for processing AVHRR data was effective as a tool in the analysis of aerosol particle characteristics. Though significant improvements were made with his study, sources of error have since been identified requiring futher improvements to his algorithm. The determination that water vapor was a significant source of error suggested a re-evaluation of the April 1982 data in order to assess water vapor impact on aerosol optical depth retrieval.

The results of this study have shown that inclusion of a water vapor correction produces a change of approximately 15% in the aerosol particle size index. Without this correction, large regions of high particle size index values, which correspond to a predominance of relatively smaller particles, were actually regions of lower values masked by water vapor effects. This made it difficult to see true areas of small particles as they were indistinguishable from the water vapor variations.

Since the phase function algorithm is a function of S_{12}, the modification made for water vapor will affect the phase function. It has been shown that the shape of the modified phase function is similar to the one determined by Frost. The improved parameterization cannot be directly compared to Frost's until the integration (3.2) is accomplished.

The aerosol optical depth has also been shown to be modified by the water vapor correction producing an approximate change of 5%. The observed extent and magnitude of areas of high dry optical depths was greater than the optical depths without the correction.

Additional improvements to the algorithm used are still necessary. Multiple scatter has not been fully accounted for. The assumption used to allow for single scatter only

is valid for optical depths less than about 0.2. This value was exceeded in the regions of high optical depth associated with major aerosol particle producing events such as the El Chicon eruptions. Errors in the values due to multiple scatter exist and must be corrected.

A second area for improvement would be in the determination of S_{12}. Current procedures use a ratio of channel 1/channel 2 radiances to calculate the particle size index. The preferred method is to use a ratio of channel 1/channel 2 optical depths, which requires a better knowledge of the phase function for both channels. It is the optical depth which contains information on the aerosol particles and would provide the best estimate for S_{12}. In this study the phase function and optical depths are at the channel 1 wavelength. This improvement should eliminate the banding that occurs in the Pacific basin photographs which possibly hides features of importance.

Finally, additional studies of global aerosol particle characteristics are needed. This study was limited to a single month. Studies exploring the changes that occur during a year and those consisting of a number of years by month or season would increase our understanding of the role of aerosol particles in the global climate.

REFERENCES

Bloembergen, N., C. K. Patel, and G. Pake (Chairpersons), 1987: Science and Technology of Directed Energy Weapons. Report of the American Physical Society Study Group, *Reviews of Modern Physics*, **59**, S1-S202.

Charlson, R. J., J. E. Lovelock, M. O. Andrea, and S. G. Warren, 1987: Oceanic phytoplankton, atmospheric sulfur, cloud albedo and climate. *Nature*, **325**, 655-661.

Cox, C. C., and W. Munk, 1954: Measurement of the roughness of the sea surface from photographs of the sun's glitter. *Journal of the Optical Society of America*, **44**, 838-850.

Coakley, J. A., 1976: Aerosols and the Earth's radiation budget. *Radiation in the Atmosphere*. H. J. Bolle, ed., Science Press, Princeton, NJ, 472-474.

Dalu, G., C. Prabhakara, and R. C. Lo, 1981: Improved accuracy of the remote sensing of sea surface temperature. In *Oceanography from Space*, J. F. R. Gower, ed., Plenum, New York, 109pp.

Dalu, G., 1986: Satellite remote sensing of atmospheric water vapor. *International Journal of Remote Sensing*, **7**, 1089-1097.

Durkee, P. A., 1984: The relationship between marine aerosol particles and satellite-detected radiance. Ph.D. Thesis, Colorado State University, Fort Collins, CO, US ISSN 0067-0340, 124pp.

Durkee, P. A., D. R. Jensen, E. E. Hindman, and T. H. Vonder Haar, 1986: The relationship between marine aerosols and satellite detected radiance. *Journal of Geophysical Research*, **91**, 4063-4072.

Durkee, P. A., F. Pfeil, E. Frost, and R. Shema, 1991: Global analysis of aerosol particle characteristics. *Atmospheric Environment*, **25A-11**, 2457-2471.

Fleagle, R. W. and J. A. Businger, 1980: *An Introduction to Atmospheric Physics*, Academic Press, New York, NY, 432pp.

Frost, E. M., 1988: Global scale estimates of aerosol particle characteristics. Master's Thesis, Naval Postgraduate School, Monterey, CA, 1-41.

Griggs, M.,1975: Measurement of atmospheric aerosol optical thickness o.er water using ERTS-1 data. *Journal of Atmospheric Pollution Control Association*, **25**, 622-626.

Jensen, J. R.,1986: *Introductory Digital Image Processing; A Remote Sensing Approach*. Prentice-Hall, Englewood Cliffs, NJ, 379pp.

Kidwell, K. B., 1986: *NOAA Polar Orbiter Data Users Guide*. NOAA NESDIS National Climatic Data Center, Satellite Data Service Division,145pp.

Lenoble, J.,1985: *Radiative Transfer in Scattering and Absorbing Atmosphere: Standard Computional Procedures.*, A. Deepak Pub., Hampton, VA, 300pp.

Mahony, T. P., 1991: Water vapor influence on satellite-measured aerosol characteristics. Master's Thesis, Naval Postgraduate School, Monterey, CA, 1-38.

Pfeil, F. R., 1986: Developing a physical basis for an aerosol climatology of the pacific ocean. Master's Thesis, Naval Postgraduate School, Monterey, CA, 76pp.

Ramsey, R. C., 1968: Study of the Remote Measurement of Ocean Color. Final Report, TRW, NASW-1658.

Weiss, R., R.J. Charlson, A. P. Waggoner, M. B. Baker, D. Cover, D. Thorsell and S. Yuen, 1976: Application of directly measured aerosol radiative properties to climate models. *Radiation in the Atmosphere* H. J. Bolle, ed., Science Press, Princeton, NJ, 469-471.

Zaitseva, N. A., 1976: The spatial-temporal variability in long-wave radiation fields at the GATE-74 grounds. *Radiation in the Atmosphere* . H. J. Bole, ed., Science Press, Princeton, NJ, 530-532.

INITIAL DISTRIBUTION LIST

		No. Copies
1.	Defense Technical Information Center Cameron Station Alexandria, VA 22304-6145	2
2.	Library, Code 52 Naval Postgraduate School Monterey, CA 93943-5002	2
3.	Chairman (Code MR/Hy) Department of Meteorology Naval Postgraduate School Monterey, CA 93943-5000	1
4.	Professor Phillip A. Durkee (Code MR/De) Department of Meteorology Naval Postgraduate School Monterey, CA 93943-5000	2
5.	Professor Patricia M. Pauley (code MR/Pa) Department of Meteorology Naval Postgraduate School Monterey, CA 93943-5000	1
6.	LT Mary B. Clifford Fleet Numerical Oceanography Center Monterey, CA 93943-5005	1
7.	Commander Naval Oceanography Command Stennis Space Center MS 39529-5000	1
8.	Commanding Officer Fleet Numerical Oceanography Center Monterey, CA 93943-5005	1
9.	Commanding Officer Naval Oceanographic and Atmospheric Research Laboratory Stennis Space Center MS 39529-5004	1
10.	Director Naval Oceanographic and Atmospheric Research Laboratory Monterey, CA 93943-5006	1

11. Chief of Naval Research
800 North Quincy Street
Arlington, VA 22217 — 1

12. Office of Naval Research
Naval Ocean Research and Development Activity
800 N. Quincy Street
Arlington, VA 22217 — 1